Electronic Supplementary Information

Partially Reduced Ru/RuO_2 Composites as Efficient and pH-Universal Electrocatalysts for Hydrogen Evolution

Yanliu Dang,[a] Tianli Wu,[b] Haiyan Tan,[a] Jinlong Wang,[c] Can Cui,[a] Peter Kerns,[d] Wen Zhao,[a] Luisa Posada,[d] Liaoyong Wen,*[e] and Steven L. Suib,*[a,d]

a. Institute of Materials Science, U-3136, University of Connecticut, Storrs, Connecticut 06269, United States

b. Henan Key Laboratory of Photovoltaic Materials and School of Physics & Electronics, Henan University, Kaifeng 475004, China

c. School of Resources and Environmental Engineering, Wuhan University of Technology, Wuhan 430070, China

d. Department of Chemistry, U-3060, University of Connecticut, Storrs, Connecticut 06269, United States

e. Key Laboratory of 3D Micro/nano Fabrication and Characterization of Zhejiang Province, School of Engineering, Westlake University, 18 Shilongshan Road, Hangzhou 310024, Zhejiang Province, China

* Email: steven.suib@uconn.edu, wenliaoyong@westlake.edu.cn

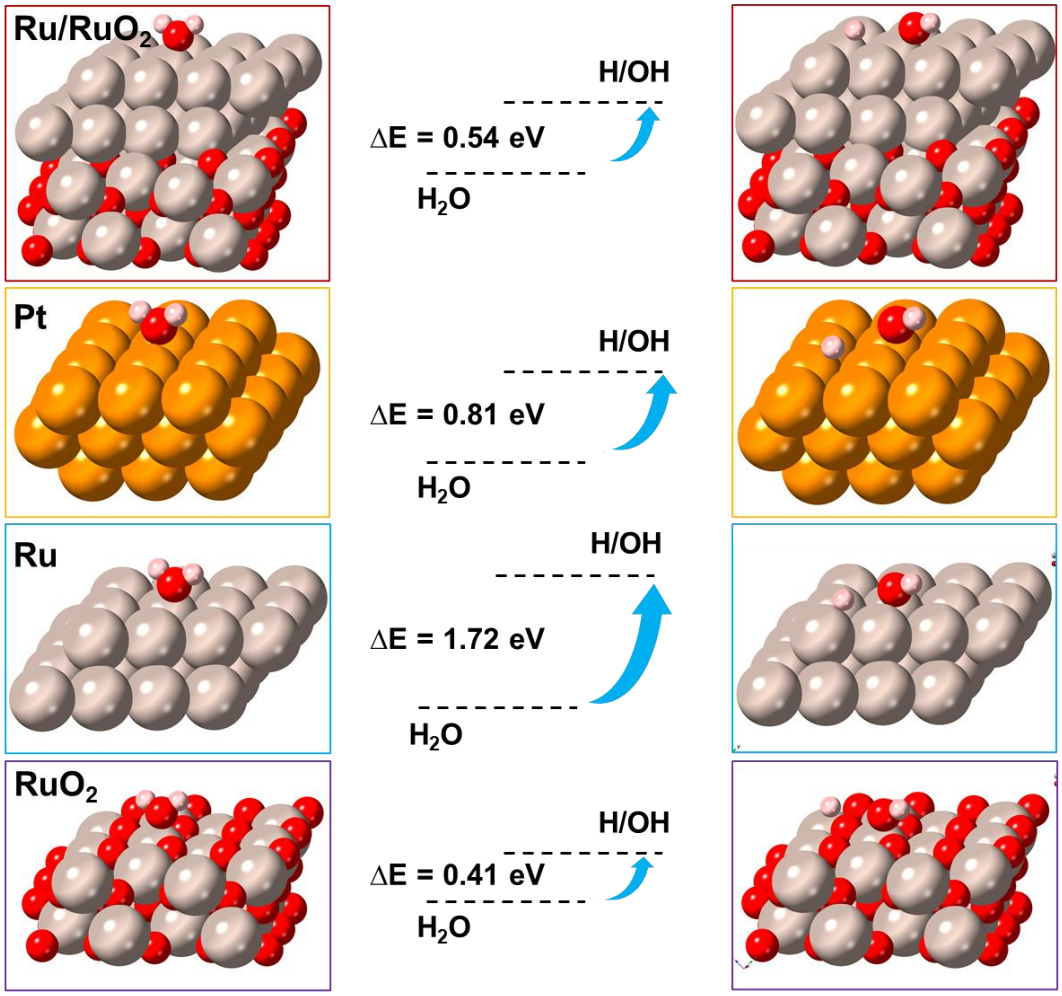

Figure S1. Adsorbed H_2O dissociation configuration on the surfaces of Ru/RuO_2, Pt, Ru, and RuO_2. Gold, grey, red and pink balls represent platinum, ruthenium, oxygen, and hydrogen atoms, respectively.

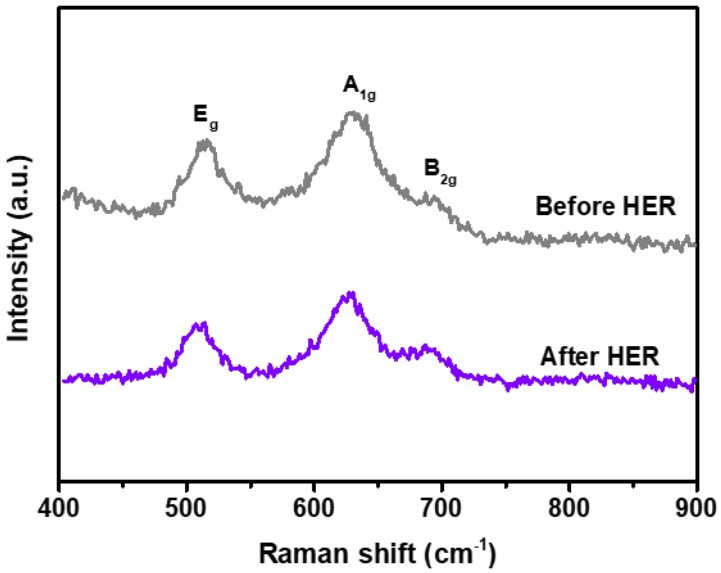

Figure S2. Raman spectra of RuO_2-300Ar prior to and post HER in 1 M KOH.

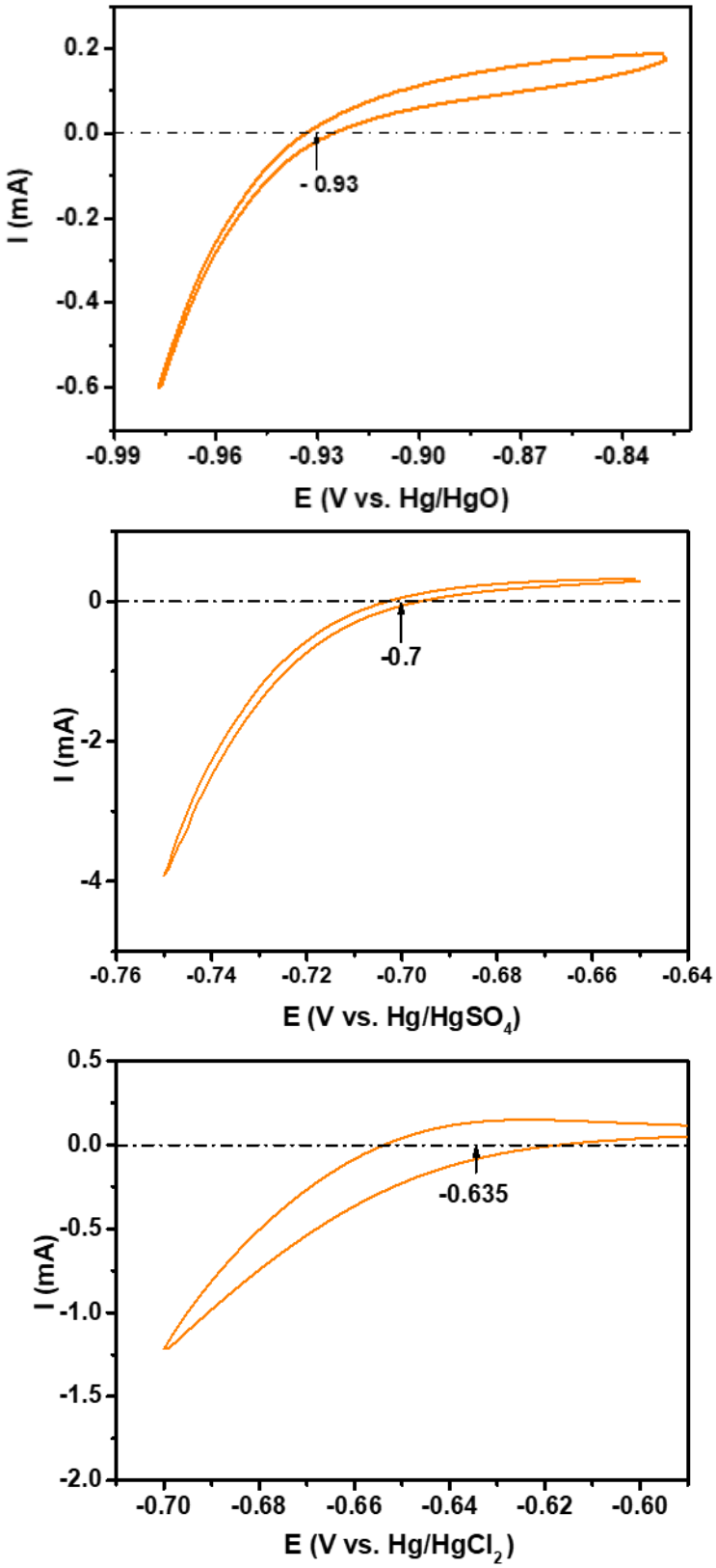

Figure S3. RHE calibration: Hg/HgO, KOH (1.0 M) reference electrode in 1 M KOH. $Hg/HgSO_4$, K_2SO_4 (sat) reference electrode in 0.5 M H_2SO_4. $Hg/HgCl_2$, KCl (sat) reference electrode in 1 M KPi (pH=7).

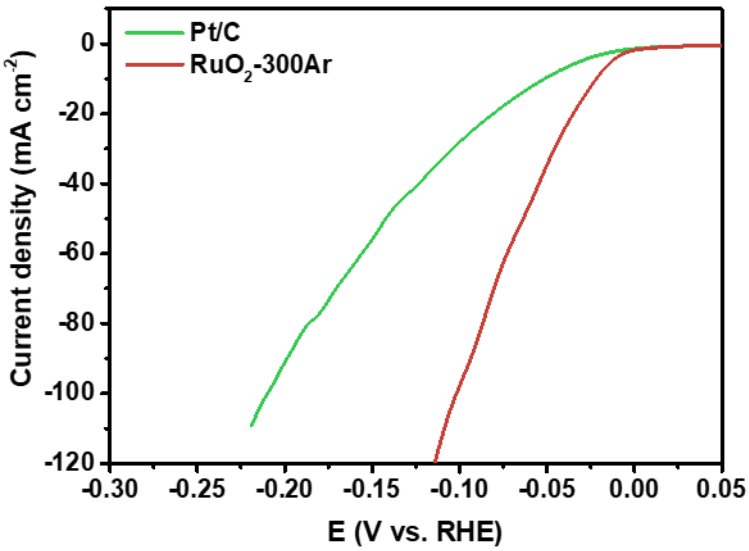

Figure S4. Polarization curves of Pt/C and RuO_2-300Ar in 1 M KOH using rotating disk electrode.

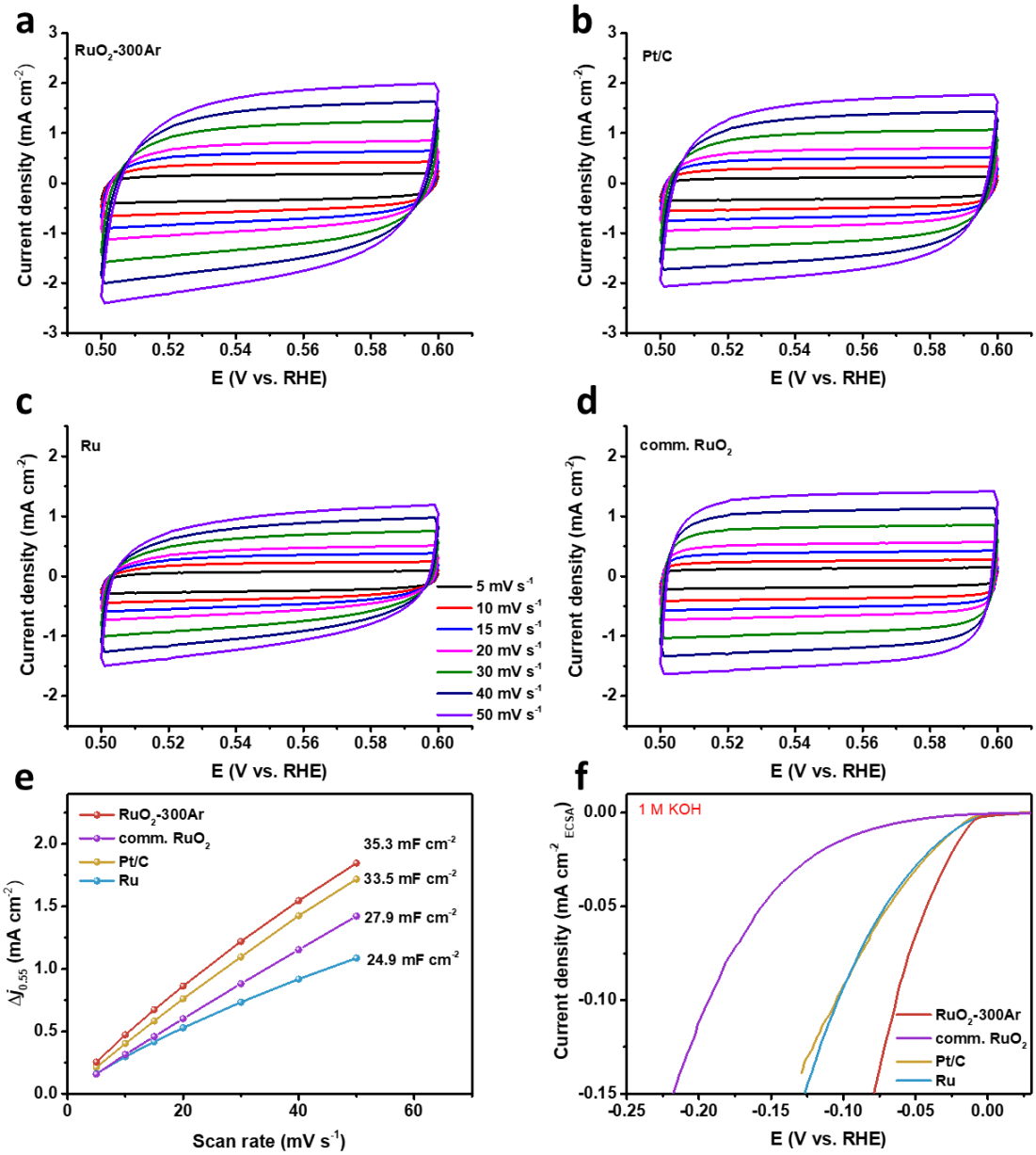

Figure S5. Cyclic voltammograms in 1 M KOH of (a) RuO_2-300Ar, (b) Pt/C, (c) Ru, and (d) comm. RuO_2 in the region of 0.5-0.6 V *vs.* RHE at various scan rates (5-50 mV s^{-1}). (e) The capacitive current densities at 0.55 V *vs.* RHE as a function of scan rate of Ru, Pt/C, commercial RuO_2, and RuO_2-300Ar derived from (a-d). (f) ESCA-normalized polarization curves of Ru, Pt/C, comm. RuO_2 and RuO_2-300Ar in 1 M KOH.

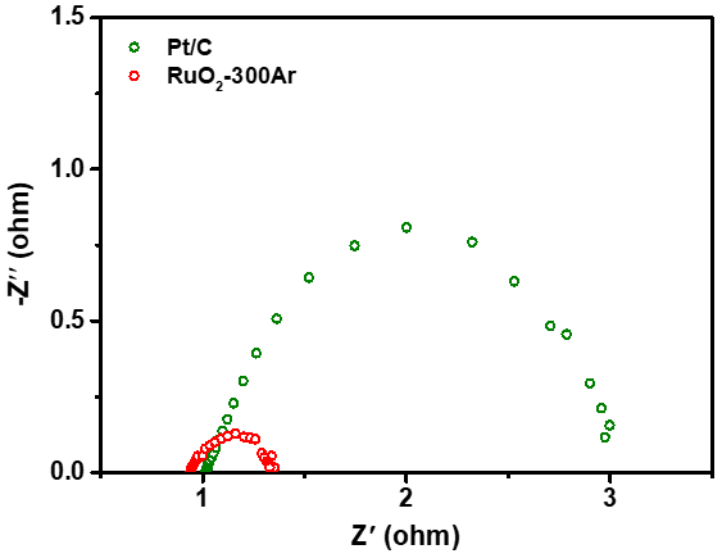

Figure S6. Electrochemical impedance spectroscopy (EIS) curves of Pt/C and RuO_2-300Ar in 1 M KOH at an overpotential of 50 mV.

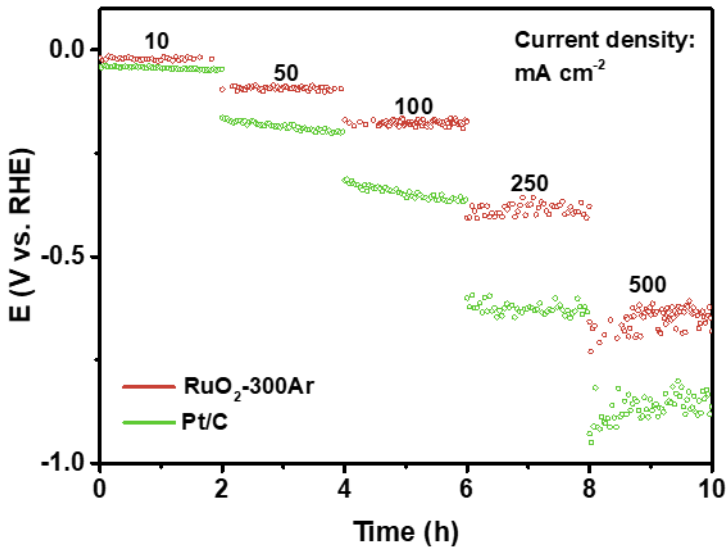

Figure S7. Multi-current chronopotentiometric curves obtained with the RuO_2-300Ar and Pt/C electrode for stability tests in 1 M KOH.

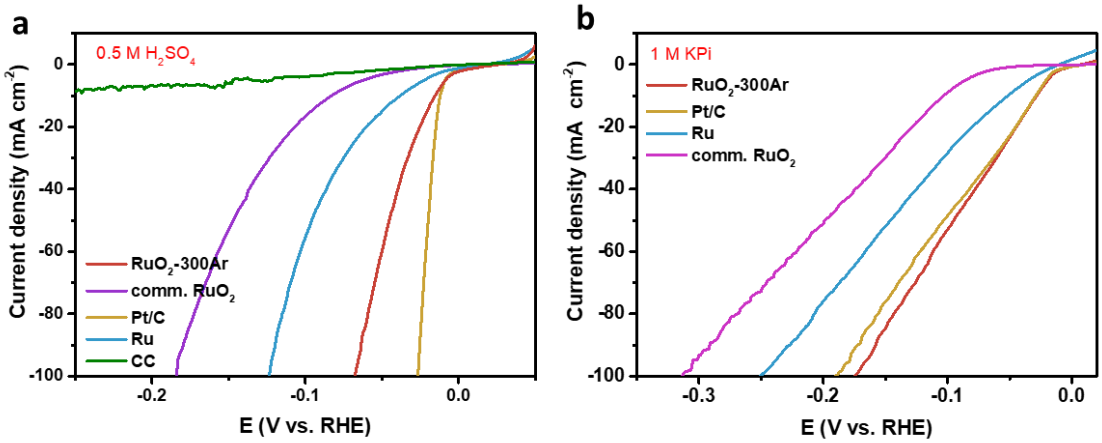

Figure S8. Polarization curves of bare CC, Ru, Pt/C, commercial RuO_2, and RuO_2-300Ar in 0.5 M H_2SO_4 (a) and 1 M KPi (b).

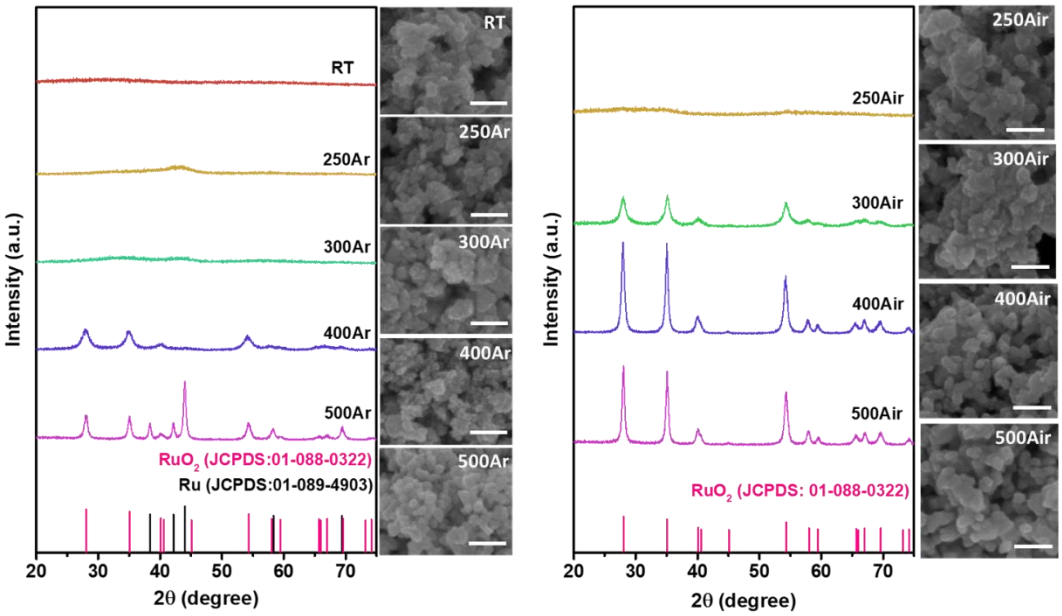

Figure S9. XRD patterns and SEM images of various RuO_2 annealed under Ar and air at multiple temperatures: 250, 300, 400, and 500 °C. Scale bar: 100 nm

The sample tags are expressed in terms of temperature and atmosphere, like 300Ar for short of RuO_2-300Ar. The as-prepared sample and samples annealed at 250Ar and 300Ar are aggregated nanoparticles with a diameter of 50-100 nm as revealed from the SEM images. The crystallization temperature under Air is lower than that under Ar. Only RuO_2-250Air is amorphous and 300Air presents similar diffraction intensity with 400Ar. The diffraction peaks of 400Air and 500Air are much higher and narrower than that of 400Ar and 500Ar, indicating a better crystallization.

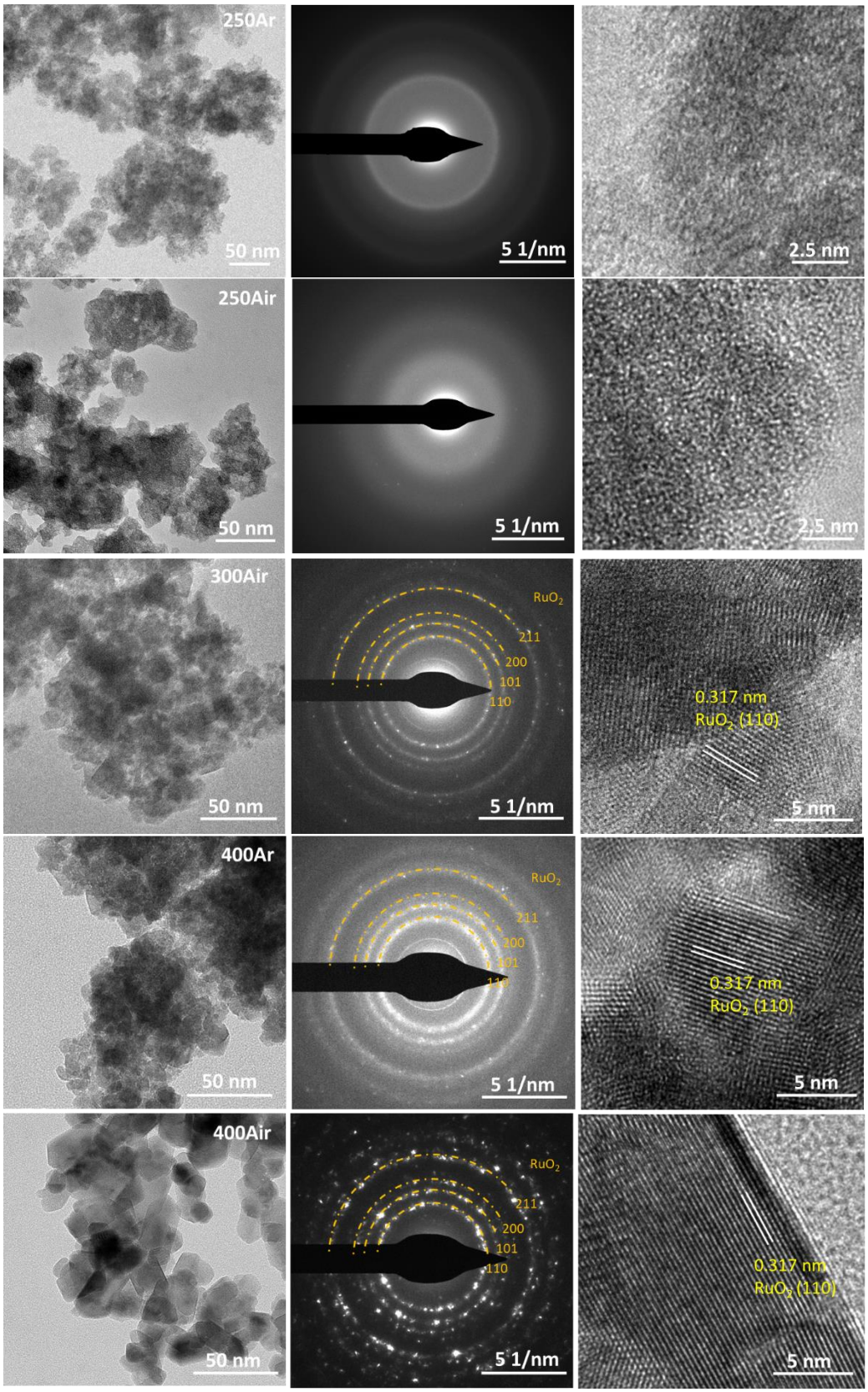
250Ar
50 nm
5 1/nm
2.5 nm
250Air
50 nm
5 1/nm
2,5 nm
300Air
50 nm
RuO2
211
200
101
110
5 1/nm
0.317 nm
RuO2 (110)
5 nm
400Ar
50 nm
RuO2
211
200
101
110
5 1/nm
0.317 nm
RuO2 (110)
5 nm
400Air
50 nm
RuO2
211
200
101
110
5 1/nm
0.317 nm
RuO2 (110)
5 nm

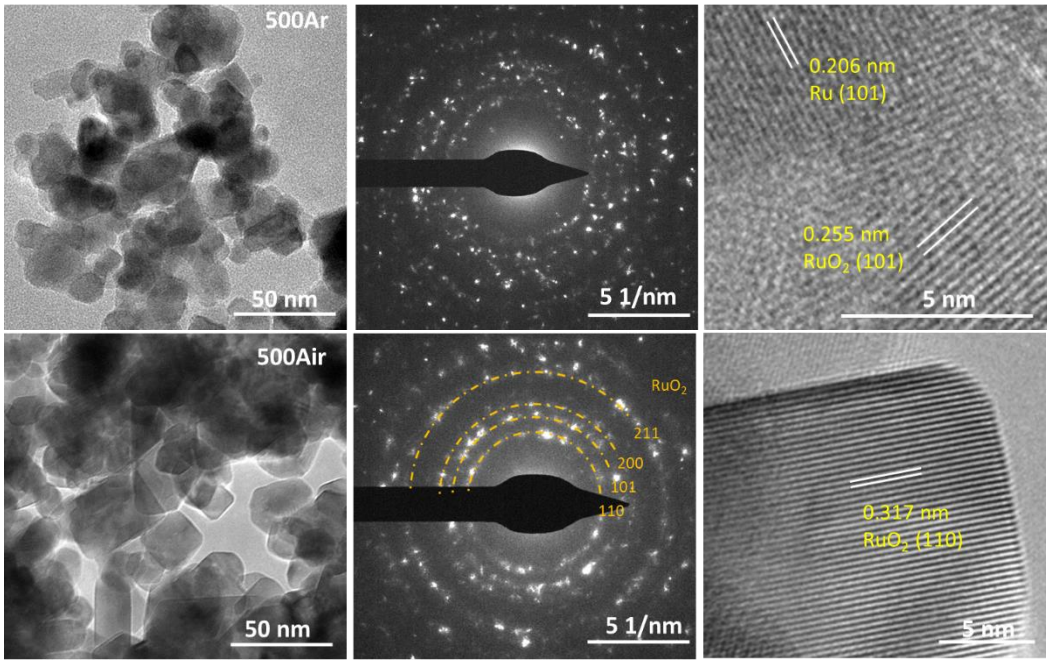

Figure S10. TEM images, SAED patterns, and HRTEM images of various RuO_2 annealed under Ar and air at multiple temperatures: 250, 300, 400 and 500 °C.

TEM coupled with SAED pattern and HRTEM was performed to investigate the morphology, particle size, crystal structure, and lattice of all RuO_2 samples. As shown in Figure S10, the morphology of RuO_2 annealed at 250Ar, 250Air, 300Ar, 300Air, and 400Ar is aggregated nanoparticles with unclear edges. As the temperature increased to 500Ar, 400Air, and 500Air, the nanoparticles with rod or cubic shapes and clear edges are observed, indicating the increase in crystallization. The SAED pattern of RuO_2 at 250Ar, 250Air, and 300Ar exhibits halo rings, suggesting the amorphous structure for these samples. RuO_2 at 300Air, 400Ar, 400Air, and 500Air reveal d-spacing values corresponding to RuO_2 planes (110), (101), (200) and (211), respectively. RuO_2-500Ar shows a complicated SAED pattern with mixed d-spacing attributed to RuO_2 and Ru. The HRTEM images provide similar results for RuO_2 samples. The random distribution of atoms is seen in 250Ar, 250Air, and 300Ar, whereas lattice spacing of 0.317 nm belongs to RuO_2 is present in all the others. In RuO_2-500Ar, the lattice spacing of 0.206 nm ascribed to Ru appears due to the reduction of RuO_2 under inert conditions.

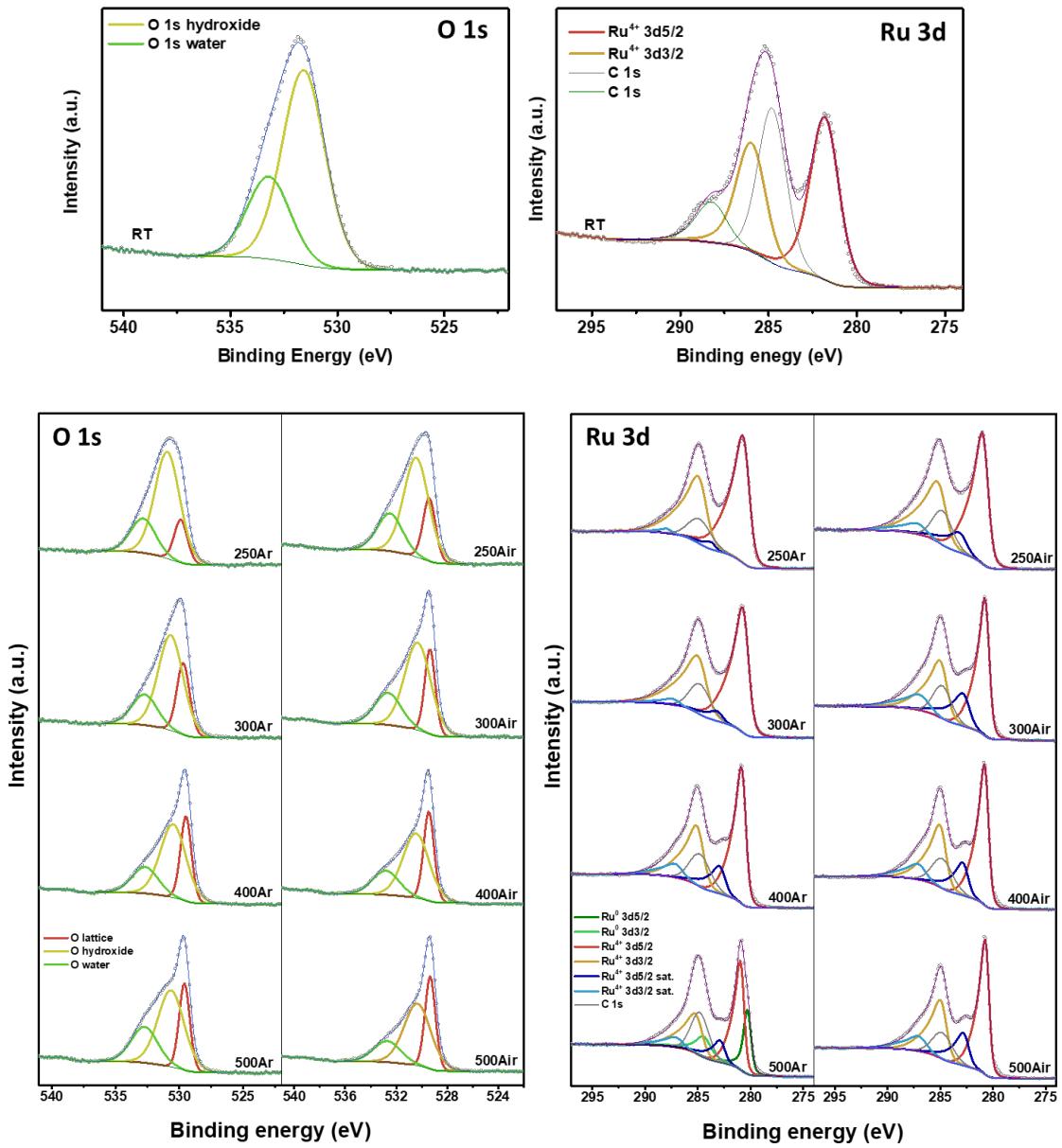

Figure S11. High-resolution O 1s and Ru 3d XPS spectra of all RuO_2 materials annealed under Ar and air at multiple temperatures: RT, 250, 300, 400, and 500 °C. The detailed peak position and percentage are shown in Table S5-S8.

XPS was carried out to analyze the electron structure and shown in Figure S11. The deconvolution results were done using CasaXPS (v2.1.0.1), with the background subtraction as described by Shirley. The default GL(30) line shape was employed to C 1s and O 1s. A derivative of the LF line shape was applied to Ru 3d according to the literature published by D. J. Morgan (*Surf. Interface Anal.*, 2015, **47**, 1072–107).

For the metallic peaks of Ru 3d, the following fitting parameters were applied:

(a) A Shirley background applied over the range 276 to 293 eV.

(b)An asymmetric line shape LF (0.8,1.25,500,180) for Ru $3d_{5/2}$ and LF (1.01,1.25,500,50) for Ru $3d_{3/2}$ with an SOS of 4.17eV and an area ratio of 0.67.

For the ruthenium oxide core levels, the methodology was as follows:

(a) A Shirley background applied over the range 276.0 to 293eV.

(b) An asymmetric line shape LF (0.25,1,45,280) for both Ru $3d_{5/2}$ and $3d_{3/2}$.

(c) A SOS of 4.17eV for photoelectron peaks and satellites with an area ratio of 0.67.

(d) Satellites 1.9-2.0 eV above each Ru 3d signal and line shape equivalent to the parent peak.

The O 1s region is assigned to lattice oxygen (O^{2-}), surface hydroxide (OH^-), and adsorbed water (H_2O), which are located at 529.5 ± 0.5, 530.5 ± 0.5 and 532.5 ± 0.5 eV, respectively. The as-prepared sample (RT) is mainly composed of hydroxide (70.26%) and water (29.74%) because of the chemical nature of $Ru(OH)_3$. As the annealing temperature rises, the amount of O^{2-} increases, whereas the amount of H_2O and OH^- decreases for samples obtained from both Ar and Air as present in Tables 7 and 8. Due to the loss of oxygen, a deviation value is seen for 500Ar (23.77%) compared to 400Ar (26.61%). As seen in Ru 3d region (Figure S11, Table 5, 6), RuO_2-RT displays one spin-orbit doublet at 281.75 eV (Ru $3d_{5/2}$) and 285.92 eV (Ru $3d_{3/2}$), The binding energy shifts to the lower values after calcination, for instance 280.54 eV (Ru $3d_{5/2}$) and 284.71 eV (Ru $3d_{3/2}$) for 300Ar. And the core level spectra of Ru 3d appear sharper with the increase of temperature. The second doublet (satellite peaks due to final state screening effects) are negligible for amorphous 250Ar and 300Ar. However, the satellite peaks at 282.74 eV (Ru $3d_{5/2}$) and 286.91 eV (Ru $3d_{3/2}$), are considerable for crystalline 400Ar. Also, it is true with 500Ar, and RuO_2 calcined above 250 °C under Air. Additionally, the third doublet, centered at 280.26 eV (Ru $3d_{5/2}$) and 284.43 eV (Ru $3d_{3/2}$), is exhibited only in 500Ar and ascribed to the metal Ru.

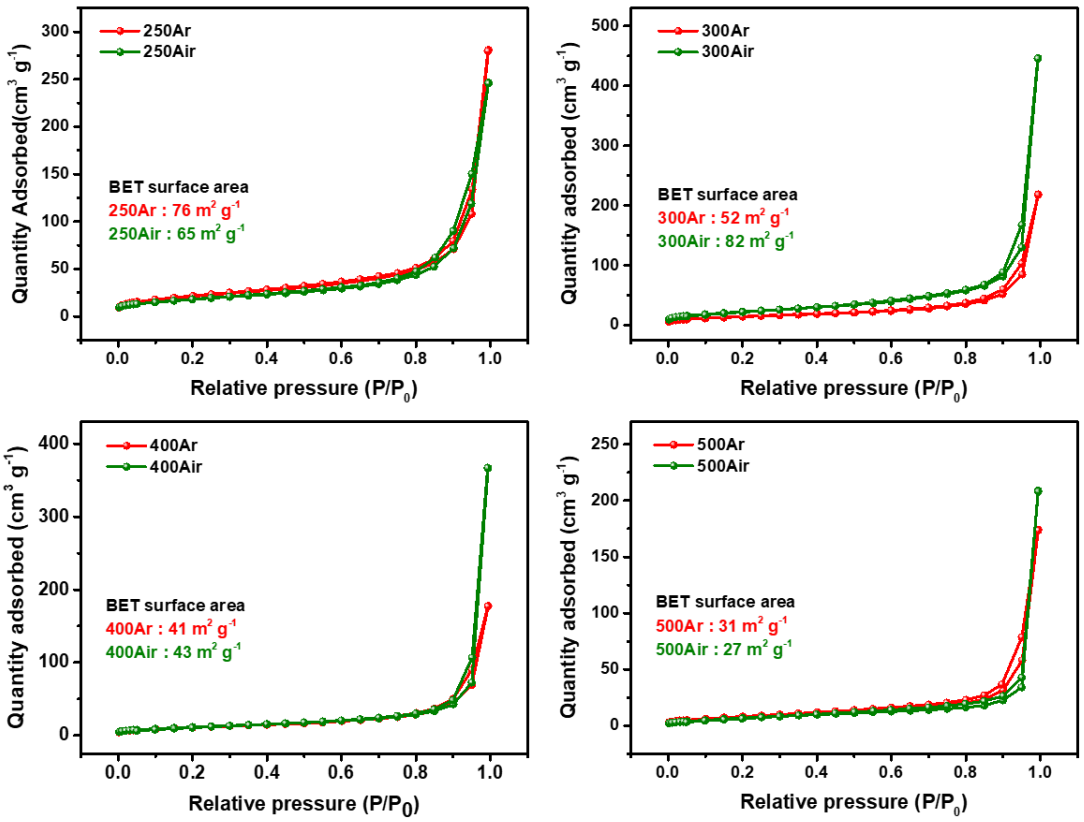

Figure S12. N_2 adsorption/desorption isotherms of all RuO_2 materials annealed under Ar and air at multiple temperatures: 250, 300, 400, and 500 °C.

The N_2 sorption and Brunauer-Emmett-Teller (BET) method were performed to study the surface areas. The isotherm curves can be attributed to Type II, which suggests the obtained RuO_2 are nonporous materials. With the temperature rising from 250 to 500 °C, the surface area decreases from 76 to 31 $m^2\ g^{-1}$ with a descent rate around 10 $m^2\ g^{-1}$ for each temperature increment. Notably, it does not show much difference in the surface area between samples under Ar or Air at the same temperature.

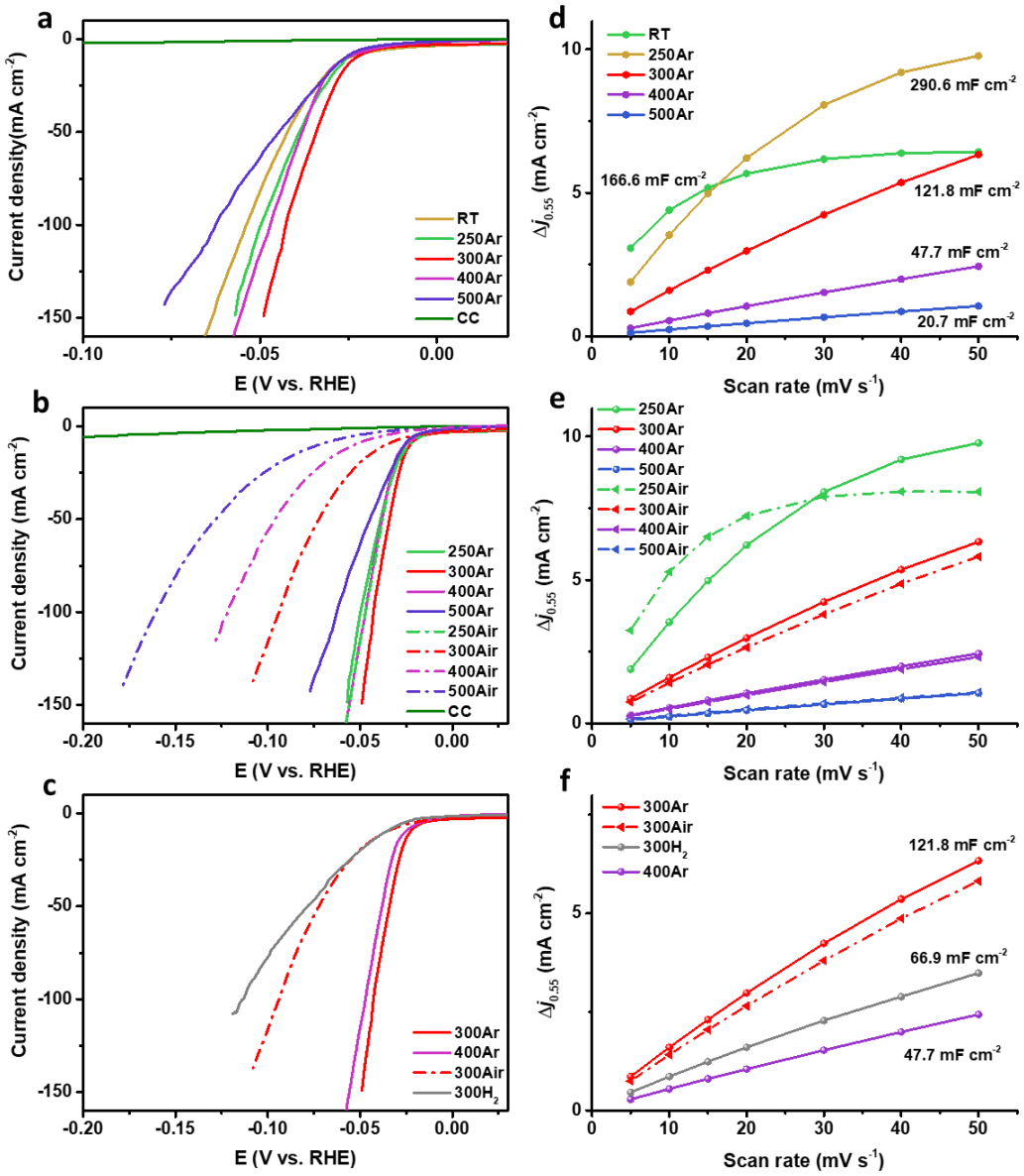

Figure S13. (a, d) Polarization curves (a) and corresponding capacitive currents at 0.55 V *vs.* RHE plotted against the scan rates (d) for bare CC and various RuO_2 annealed under Ar at multiple temperatures in 1 M KOH. (b, e) Polarization curves (b) and corresponding capacitive currents at 0.55 V *vs.* RHE plotted against the scan rates (e) of RuO_2 annealed under Ar compared with that under Air in 1 M KOH. (c, f) Polarization curves (c) and corresponding capacitive currents at 0.55 V *vs.* RHE plotted against the scan rates (f) of RuO_2-300H_2 compared with RuO_2-300Ar, 300Air, and 400Ar in 1 M KOH.

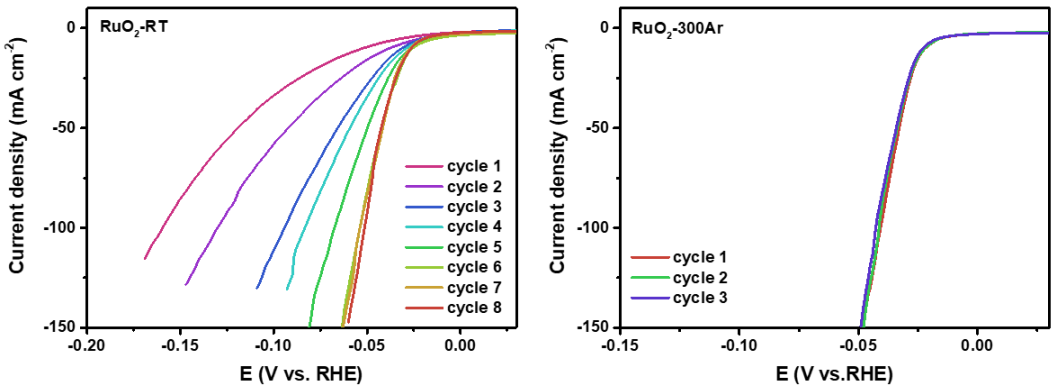

Figure S14. Activation study of RuO_2-RT and RuO_2-300Ar toward HER in 1 M KOH: polarization curves records from the beginning to the stable status without activation.

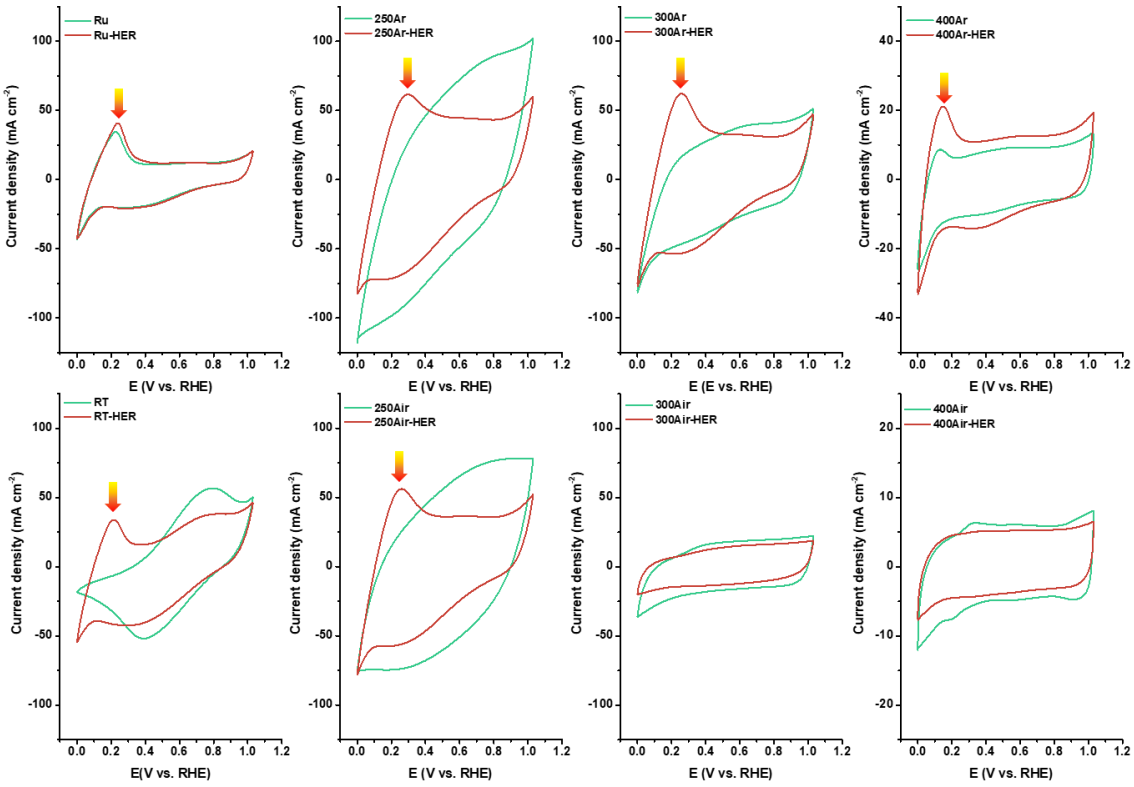

Figure S15. Cyclic voltammogram in the range of 0-1.03 V *vs.* RHE of RuO_2-300H_2 (Ru), 300Ar, 300Air, 250Ar, 250Air 400Ar, and 400Air prior to and post HER in 1 M KOH.

Pure RuO_2 shows a rectangular shape of CV, including RuO_2-300Air and 400Air. For the amorphous RuO_2-250Ar, 250Air, a similar hydrogen oxidation peak shows up after HER, indicating the reduction of RuO_2 and the existence of metal Ru. Moreover, the CV data show the hydrogen oxidation peak is present for RuO_2-400Ar before the HER, which is similar to the reduced RuO_2-300Ar after the HER and clearly different from RuO_2-400Air. This suggests that RuO_2-400Ar may contain trace amounts of metal and possess mixed properties of oxides and metals.

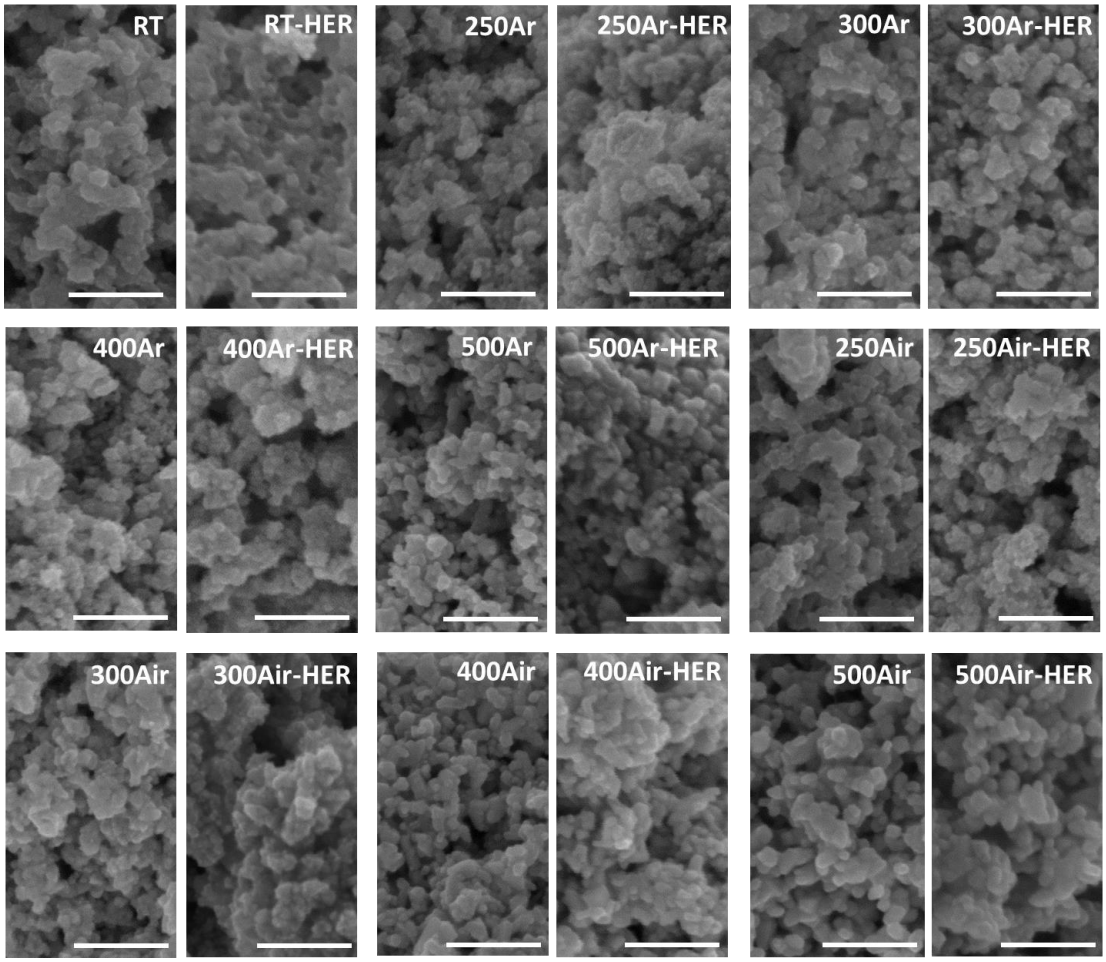

Figure S16. SEM images of all RuO_2 materials annealed under Ar and air at multiple temperatures: RT, 250, 300, 400, and 500 °C prior to and post HER in 1 M KOH. Scale bar: 200 nm

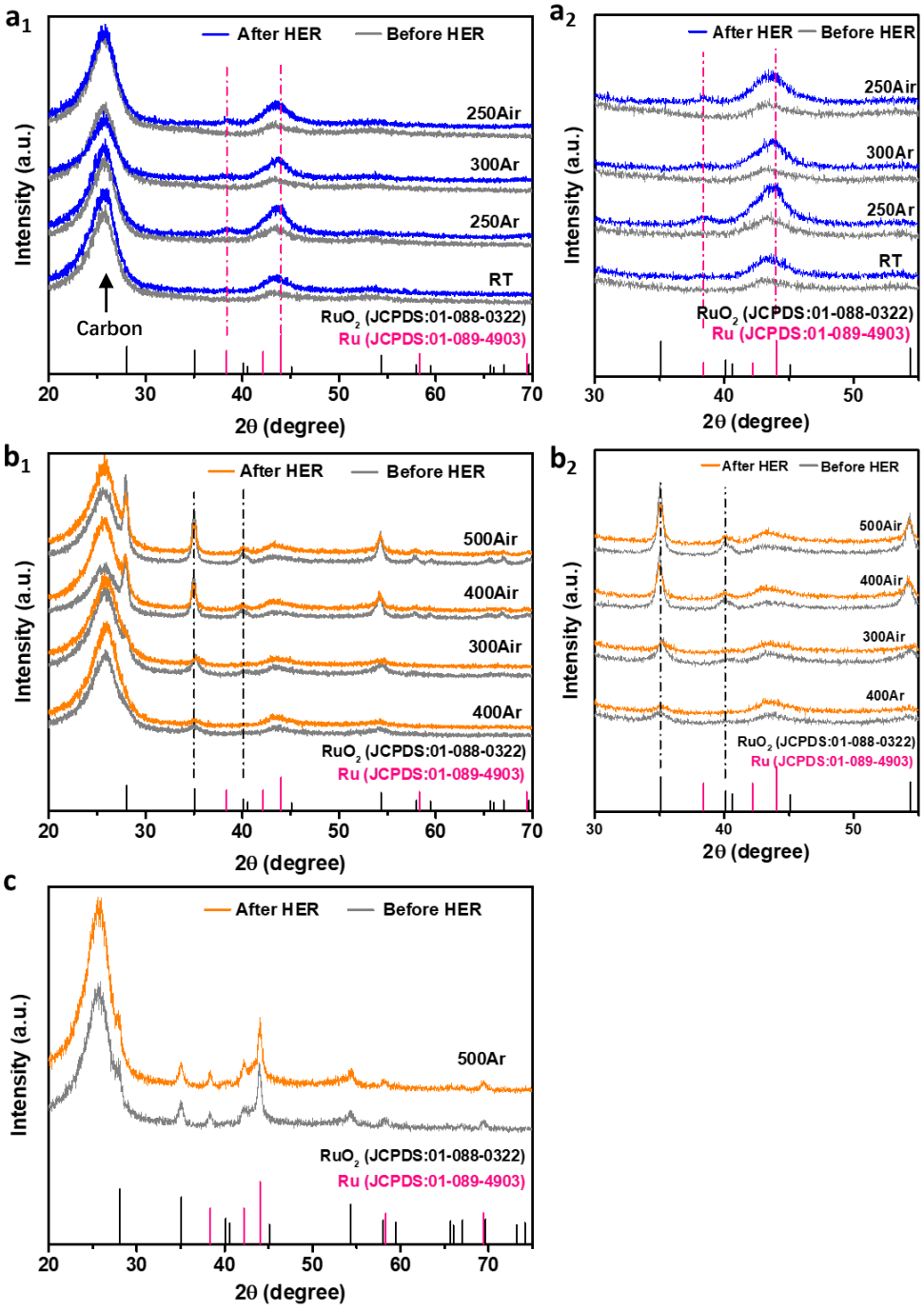

Figure S17. XRD patterns of all RuO_2 materials prior to and post HER in 1 M KOH: (a) amorphous RuO_2 including RuO_2-RT, 250Ar, 300Ar, and 250Air. (b) crystallized RuO_2 materials including RuO_2-400Ar, 300Air, 400Air, and 500Air. (c) RuO_2-500Ar. Based on the structural changes, RuO_2 samples are divided into two categories. New peaks attributed to Ru metal show up in the XRD patterns of the amorphous RuO_2 samples including as-obtained RT, 250Ar, 300Ar, and 250Air after HER (Figure S17a). Whereas the XRD patterns maintain almost the same after HER for the crystallized RuO_2, such as 300Air, 400Ar, 400Air, 500Ar, and 500Air (Figure S17b, c).

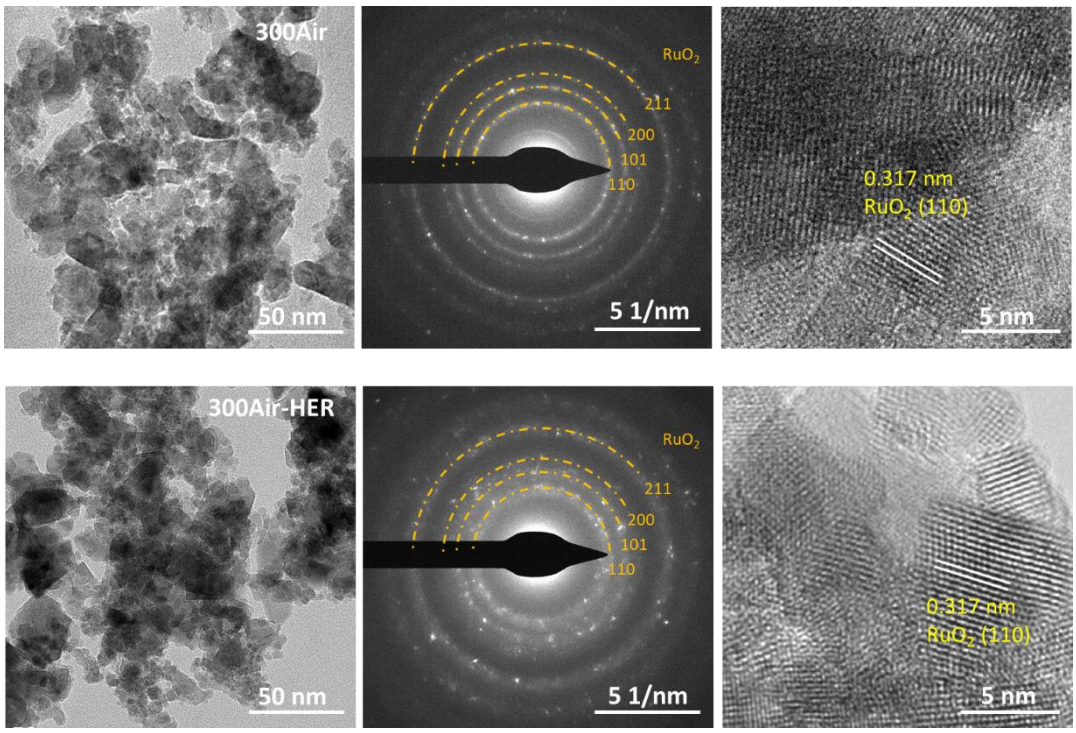

Figure S18. TEM images, SAED patterns and HRTEM images of RuO_2-300Air prior to and post HER in 1 M KOH.

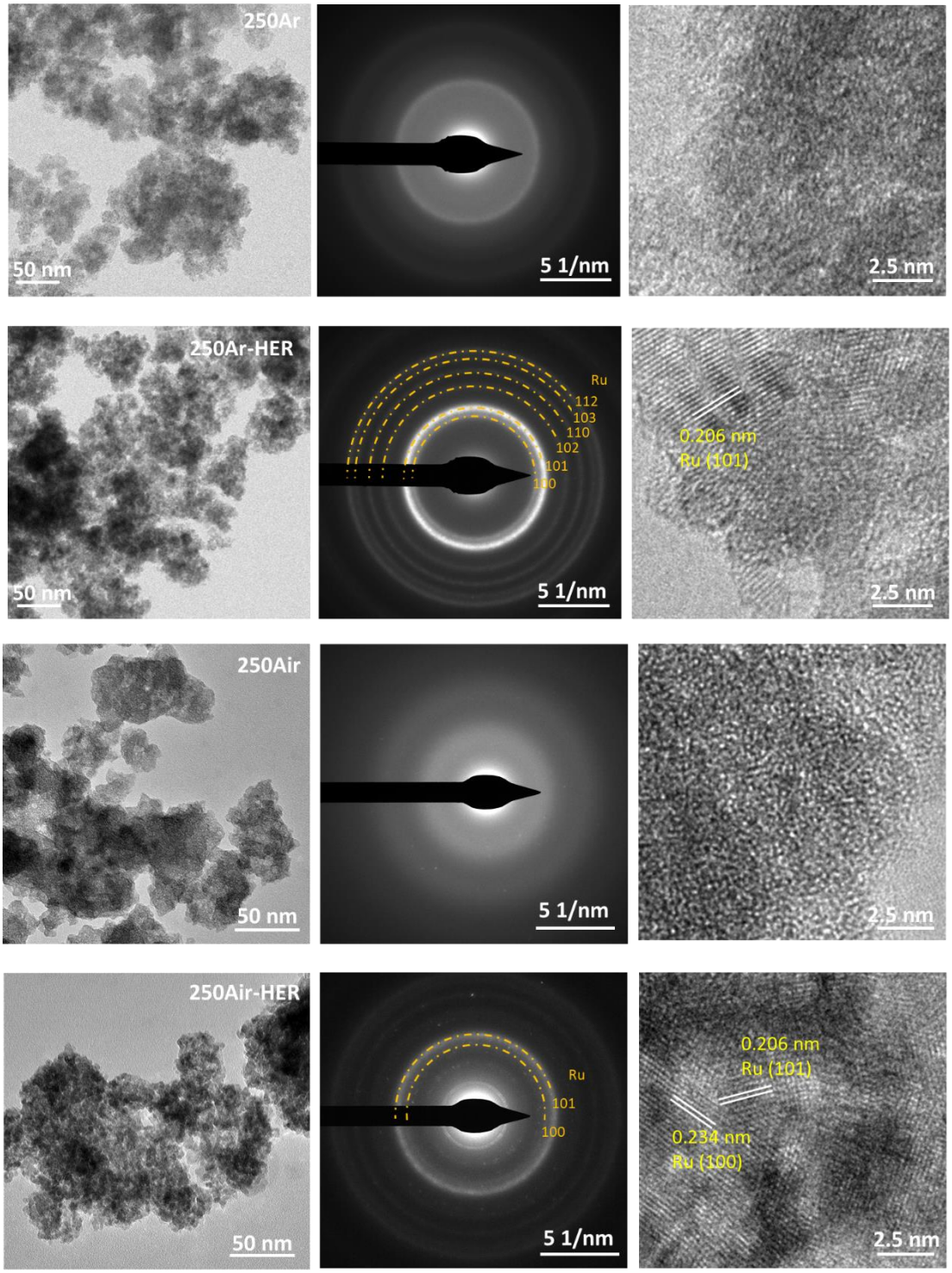

Figure S19. TEM images, SAED patterns and HRTEM images of those amorphous RuO_2 materials including RuO_2-250Ar and 250Air prior to and post HER in 1 M KOH. The ring patterns with d-spacing values corresponding to Ru planes (100), (101), (102), (110), (103) and (112) show up in the SAED patterns of the amorphous RuO_2 samples after HER. The HRTEM images reveal the lattice spacings of 0.206 and 0.234 nm belonging to Ru (101) and (100) facets, respectively.

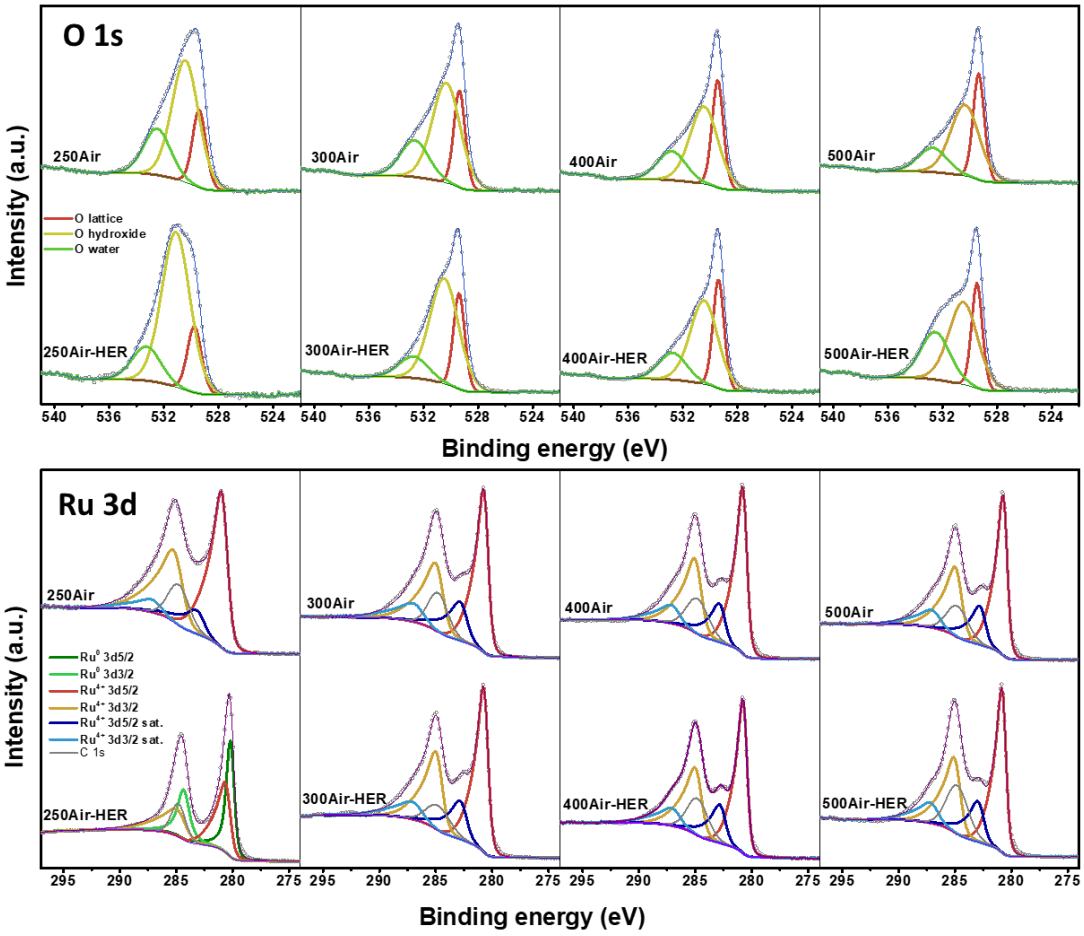

Figure S20. High-resolution O 1s and Ru 3d XPS spectra with deconvolution curves of RuO_2 materials under Air at multiple temperatures prior to and post HER in 1 M KOH.

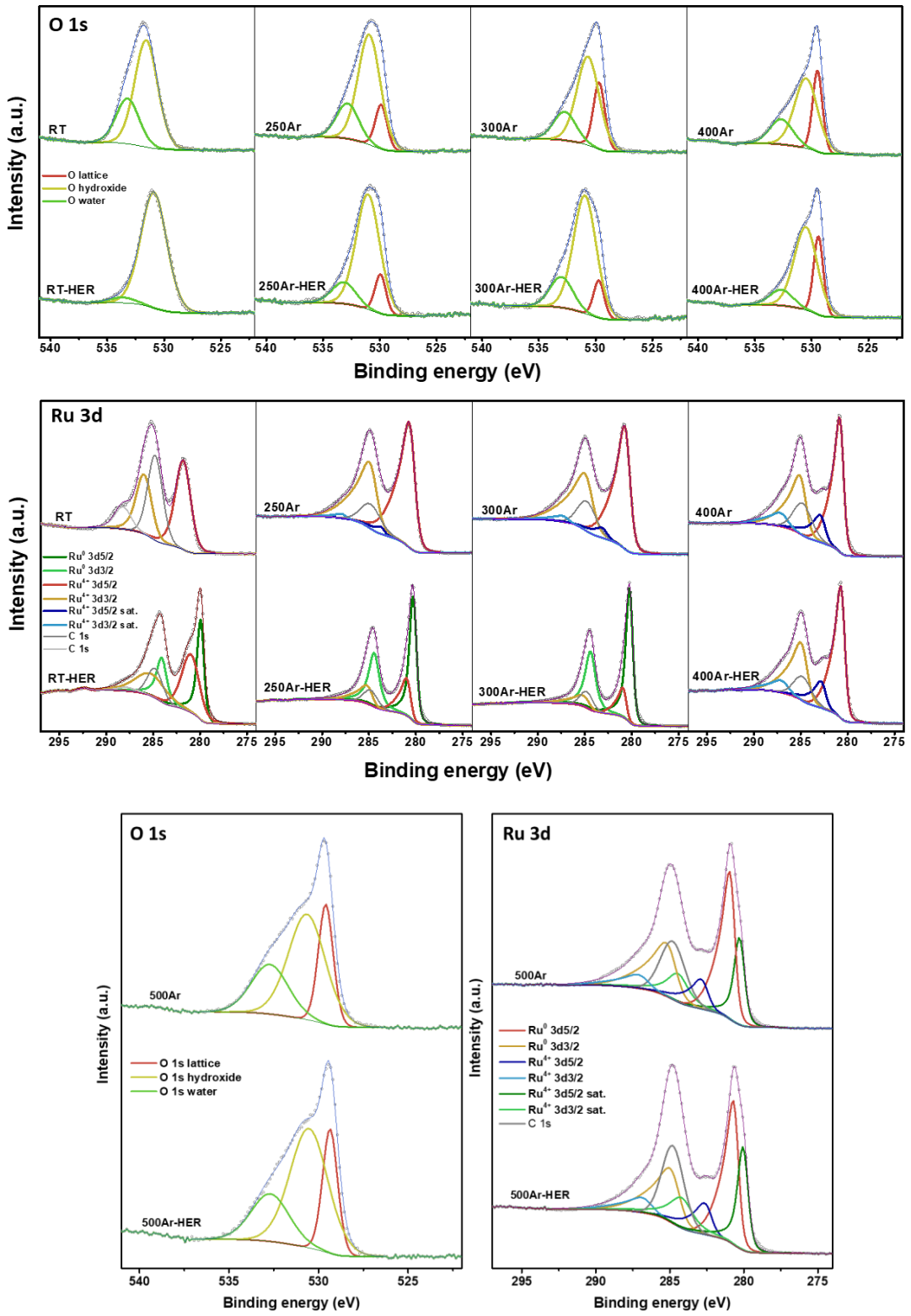

Figure S21. High-resolution O 1s and Ru 3d XPS spectra with deconvolution curves of RuO_2 materials under Ar at multiple temperatures prior to and post HER in 1 M KOH.

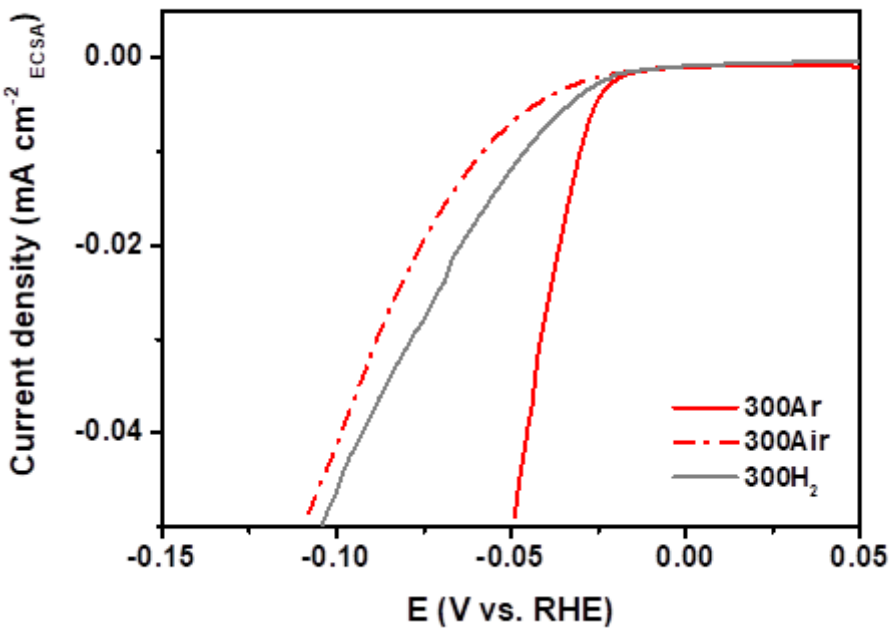

Figure S22. ESCA-normalized polarization curves of RuO_2 annealed at 300Ar, 300Air, and 300H_2 in 1 M KOH.

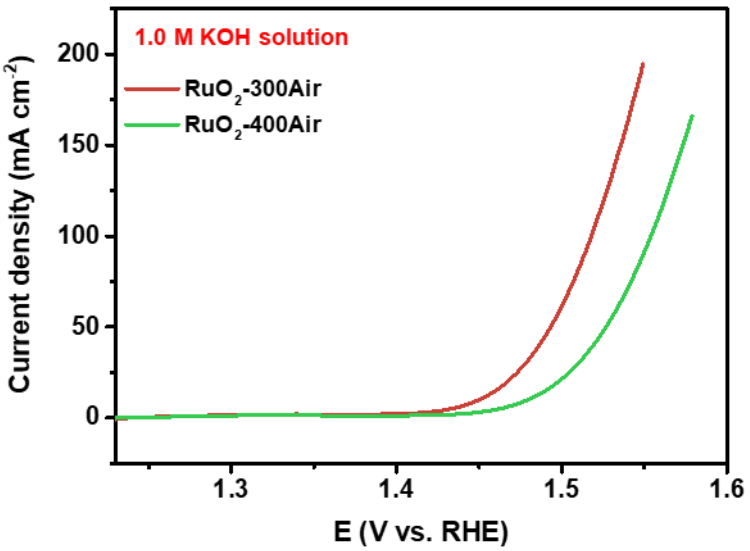

Figure S23. Polarization curves of RuO_2-300Air and 400Air toward OER in 1 M KOH.

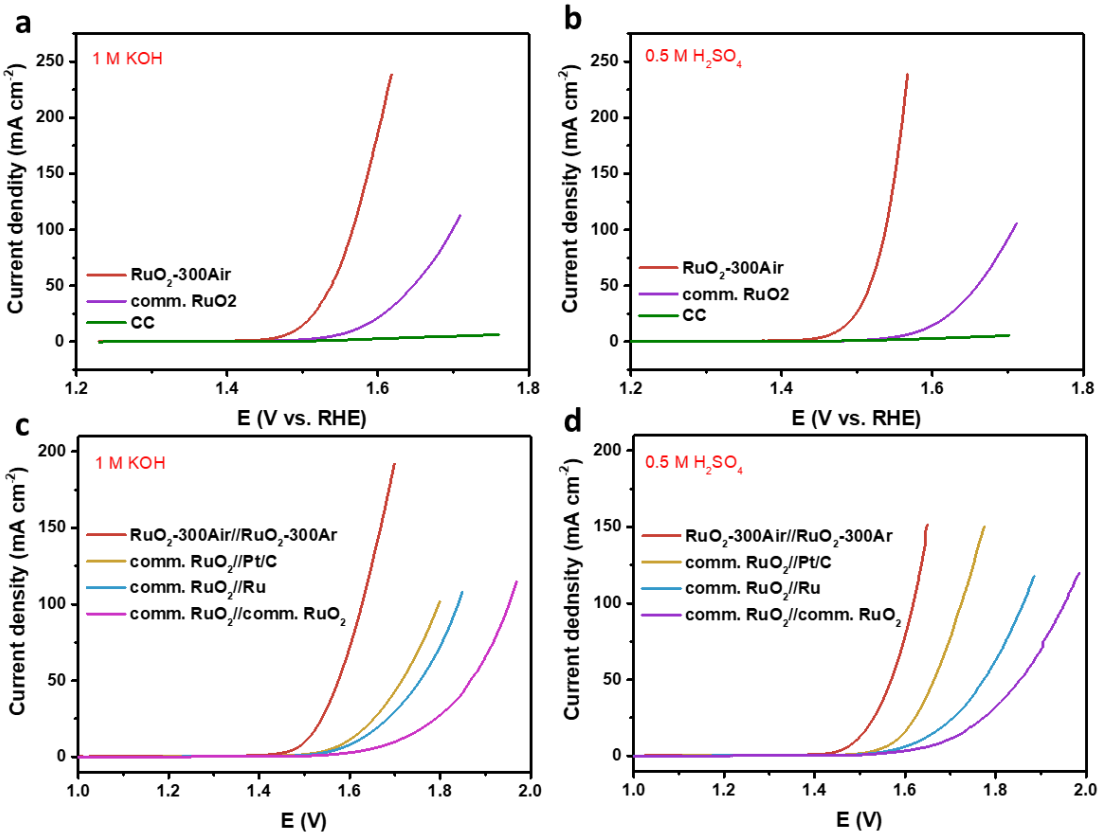

Figure S24. (a, b) Polarization curves of bare CC, commercial RuO_2, and RuO_2-300Air toward OER in 1 M KOH (a) and 0.5 M H_2SO_4 (b). (c, d) Overall water-splitting of the electrolyzer RuO_2-300Ar//RuO_2-300Air, comm. RuO_2//Pt/C, comm. RuO_2//Ru, and comm. RuO_2//comm. RuO_2: polarization curves in 1 M KOH (c) and 0.5 M H_2SO_4 (d).

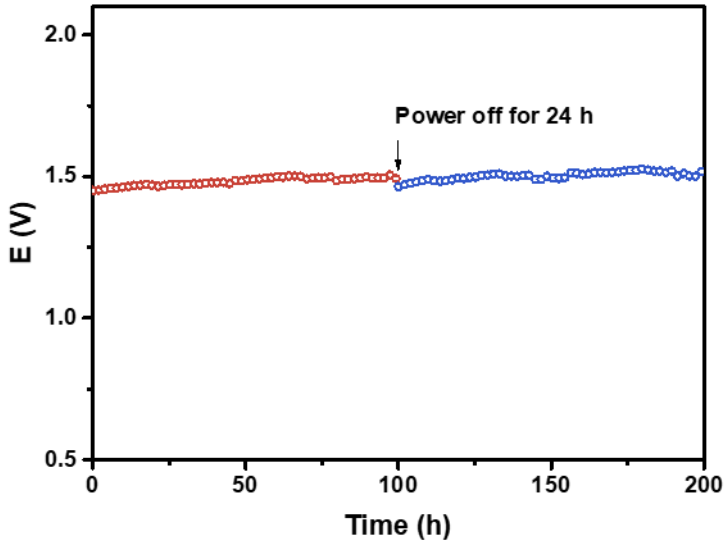

Figure S25. Long-time stability test for overall water-splitting of the electrolyzer RuO_2-300Ar//RuO_2-300Air at 10 mA cm^{-2} in 0.5 M H_2SO_4.

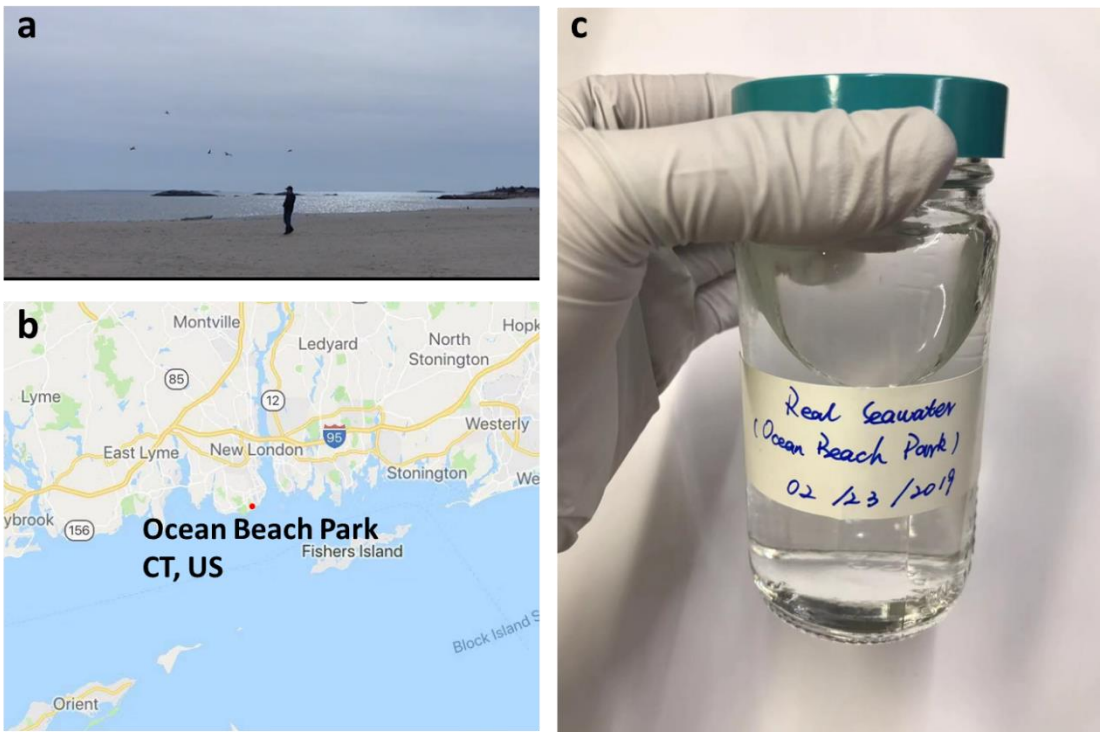

Figure S26. Collection of seawater. (a) Photograph of the Ocean Beach Park in Connecticut, United State on February 23th, 2019. (b) The location of Ocean Beach Park in Connecticut, United States (Copyright @ Google Maps). (c) Bottled seawater used for seawater HER experiments without purification and desalination.

Table S1. Summary of C_{dl} and calculated ECSA value of RuO_2-300Ar, Pt/C, Ru and comm. RuO_2 electrodes

Catalysts	C_{dl} (mF cm^{-2})	ECSA (cm^2)
RuO_2-300Ar	35.3	882.5
Pt/C	33.5	837.5
Ru	24.9	622.5
Comm. RuO_2	27.9	697.5

Table S2. Summary of C_{dl} value of pure RuO_2 electrodes annealed under Ar and Air at 250, 300, 400, and 500 ºC

Catalysts	C_{dl} (mF cm^{-2})
250Ar	290.6
250Air	269.9
300Ar	121.8
300Air	112.7
400Ar	47.7
400Air	45.6
500Ar	20.7
500Air	20.7

Table S3. Summary of atomic ratio derived from EDS of those amorphous RuO_2 materials including RuO_2-RT, 250Ar, 300Ar, and 250Air prior to and post HER in 1 M KOH

Sample	Position	Atomic % Oxygen (O)	Atomic % Ruthenium (Ru)	Atomic ratio O : Ru
RT	1	33.34	5.90	5.6 : 1
	2	27.83	3.79	7.3 : 1
250Ar	1	19.50	9.03	2.1 : 1
	2	19.24	5.41	3.5 : 1
300Ar	1	25.42	10.97	2.3 : 1
	2	20.31	9.81	2.1 : 1
250Air	1	20.69	4.71	4.4 : 1
	2	29.91	7.91	3.8 : 1
RT-HER	1	26.74	9.61	**2.8 : 1**
	2	38.73	10.83	**3.6 : 1**
250Ar-HER	1	20.69	28.01	**0.7 : 1**
	2	19.29	26.62	**0.7 : 1**
300Ar-HER	1	17.30	14.31	**1.2 : 1**
	2	15.49	11.22	**1.4 : 1**
250Air-HER	1	11.09	6.74	**1.6 : 1**
	2	11.06	6.30	**1.7 : 1**

Table S4. Summary of atomic ratio derived from EDS of those crystallized RuO_2 materials including RuO_2-400Ar, 500Ar, 300Air, 400Air, and 500Air prior to and post HER in 1 M KOH

Sample	Position	Atomic % Oxygen (O)	Atomic % Ruthenium (Ru)	Atomic ratio O : Ru
400Ar	1	29.10	10.44	2.8 : 1
	2	27.26	8.74	3.1 : 1
500Ar	1	29.71	27.42	**1.1 : 1**
	2	27.14	20.40	**1.3 : 1**
300Air	1	35.27	10.83	3.3 : 1
	2	26.78	7.77	3.4 : 1
400Air	1	32.55	12.15	2.7 : 1
	2	35.00	10.24	3.4 : 1
500Air	1	34.48	12.86	2.7 : 1
	2	25.14	9.11	2.8 : 1
400Ar-HER	1	31.40	10.49	3.0 : 1
	2	21.69	7.74	2.8 : 1
500Ar-HER	1	26.64	21.86	**1.2 : 1**
	2	28.78	28.03	**1.0 :1**
300Air-HER	1	29.15	8.06	3.6 : 1
	2	30.66	10.03	3.1 : 1
400Air-HER	1	40.24	14.40	2.8 : 1
	2	30.39	10.76	2.8 : 1
500Air-HER	1	24.30	7.63	3.2 : 1
	2	30.75	8.68	3.5 : 1

Table S5. Summary of Ru 3d spectral fitting parameters: binding energy (eV), percentage of total area for those amorphous RuO_2 materials including RuO_2-RT, 250Ar, 300Ar, and 250Air prior to and post HER in 1 M KOH

Catalysts	Ru $3d_{5/2}$ (oxide)		Ru $3d_{3/2}$ (oxide)		Ru $3d_{5/2}$ (satellite)		Ru $3d_{3/2}$ (satellite)		Ru $3d_{5/2}$ (metal)		Ru $3d_{3/2}$ (metal)	
	Peak 1 (eV)	%	Peak 2 (eV)	%	Peak 3 (eV)	%	Peak 4 (eV)	%	Peak 5 (eV)	%	Peak 6 (eV)	%
RT	281.75	35.57	285.92	23.81								
250Ar	280.50	51.26	284.67	34.31	283.61	1.97	287.78	1.32				
300Ar	280.54	48.38	284.71	32.38	282.98	3.74	287.15	2.50				
250Air	280.80	43.82	284.97	29.33	282.97	8.48	286.87	5.68				
RT-HER	280.92	28.17	285.09	18.85					279.90	23.68	284.07	15.86
250Ar-HER	280.84	15.63	285.01	10.46					280.26	39.86	284.43	26.68
300Ar-HER	280.80	11.14	284.97	7.46					280.20	44.29	284.37	29.64
250Air-HER	280.50	25.48	284.67	17.05					280.17	27.82	284.34	18.62

Table S6. Summary of Ru 3d spectral fitting parameters: binding energy (eV), percentage of total area for those crystallized RuO_2 materials including RuO_2-400Ar, 500Ar, 300Air, 400Air, and 500Air prior to and post HER in 1 M KOH

Catalysts	Ru $3d_{5/2}$ (oxide)		Ru $3d_{3/2}$ (oxide)		Ru $3d_{5/2}$ (satellite)		Ru $3d_{3/2}$ (satellite)		Ru $3d_{5/2}$ (metal)		Ru $3d_{3/2}$ (metal)	
	Peak 1 (eV)	%	Peak 2 (eV)	%	Peak 3 (eV)	%	Peak 4 (eV)	%	Peak 5 (eV)	%	Peak 6 (eV)	%
300Air	280.61	38.55	284.78	25.80	282.64	13.49	286.81	9.03				
400Air	280.66	39.53	284.83	26.46	282.69	12.30	286.86	8.23				
500Air	280.60	39.12	284.77	26.18	282.63	13.29	286.80	8.89				
400Ar	280.70	40.58	284.87	27.16	282.74	10.67	286.91	7.14				
500Ar	280.83	28.08	285.00	18.79	282.72	7.49	286.89	5.01	280.26	14.24	284.43	9.53
300Air-HER	280.62	40.24	284.79	26.93	282.64	13.67	286.81	9.15				
400Air-HER	280.64	37.69	284.81	25.23	282.65	13.42	286.82	8.98				
500Air-HER	280.71	36.29	284.88	24.29	282.78	12.83	286.95	8.58				
400Ar-HER	280.57	43.00	284.74	28.78	282.66	10.26	286.83	6.87				
500Ar-HER	280.58	25.49	284.75	17.06	282.48	7.56	286.65	5.06	280.02	15.66	284.19	10.48

Table S7. Summary of O 1s spectral fitting parameters: binding energy (eV), percentage of total area for those RuO_2 materials obtained under Ar including RuO_2-RT, 250Ar, 300Ar, 400Ar, and 500Ar prior to and post HER in 1 M KOH

Catalysts	O 1s lattice		O 1s hydroxide		O 1s water		Ratio	
	Peak 1 (eV)	%	Peak 2 (eV)	%	Peak 3 (eV)	%	$\frac{Peak\ 1}{Peak\ 1 + Peak\ 2}$%	$\frac{Peak\ 2}{Peak\ 1 + Peak\ 2}$%
RT			531.58	70.26	533.21	29.74		
250Ar	529.88	13.89	530.94	65.20	532.84	20.90	17.56	82.44
300Ar	529.69	22.67	530.67	58.53	532.71	18.80	27.92	72.08
400Ar	529.48	26.61	530.48	53.98	532.66	19.41	33.02	66.98
500Ar	529.60	23.77	530.65	51.84	532.72	24.39	31.44	68.56
RT-HER			530.90	95.55	533.66	4.45		
250Ar-HER	529.95	11.84	531.04	74.30	533.16	13.86	13.75	86.25
300Ar-HER	529.72	10.54	530.94	71.01	533.00	18.45	12.92	87.08
400Ar-HER	529.40	24.97	530.51	63.08	532.66	11.96	28.36	71.64
500Ar-HER	529.36	22.8	530.53	55.2	532.7	22	29.23	70.77

Table S8. Summary of O 1s spectral fitting parameters: binding energy (eV), percentage of total area for RuO_2 materials obtained under Air including RuO_2-250Air, 300Air, 400Air, and 500Air prior to and post HER in 1 M KOH

Catalysts	O 1s lattice		O 1s hydroxide		O 1s water		Ratio	
	Peak 1 (eV)	%	Peak 2 (eV)	%	Peak 3 (eV)	%	$\frac{Peak\ 1}{Peak\ 1 + Peak\ 2}$%	$\frac{Peak\ 2}{Peak\ 1 + Peak\ 2}$%
250Air	529.41	18.82	530.43	58.86	532.49	22.32	24.23	75.77
300Air	529.36	22.27	530.32	56.91	532.64	20.81	28.13	71.87
400Air	529.45	28.71	530.45	51.95	532.81	19.34	35.59	64.41
500Air	529.34	30.21	530.34	52.11	532.70	17.69	36.70	63.30
250Air-HER	529.77	14.88	531.12	69.75	533.28	15.37	17.58	82.42
300Air-HER	529.39	22.97	530.47	64.02	532.73	13.00	26.41	73.59
400Air-HER	529.39	28.25	530.44	54.35	532.73	17.40	34.20	65.80
500Air-HER	529.47	23.02	530.46	48.82	532.52	28.17	32.04	67.96

Table S9. Summary of recently reported representative HER electrocatalysts in alkaline electrolytes

Catalysts	Overpotential mV@10 mA cm^{-2}	Tafel slope mV dec^{-1}	References
RuO_2-300Ar	17	35	This work
Pt_{SA}-$Co(OH)_2$@Ag NWs	29	35.72	Energy Environ. Sci. DOI: 10.1039/d0ee01347a 2020
IrP_2@NC	28	50	Energy Environ. Sci. 2019, 12 (3), 952–957
Ni NP|Ni–N–C	147	114	Energy Environ. Sci. 2019, 12, 149–156
Ni/WC@C	77	68.6	Energy Environ. Sci., 2018, 11, 2114–2123
RuCoP	23	37	Energy Environ. Sci. 2018, 11, 1819–1827
CoMoP	81	55.53	Energy Environ. Sci., 2017, 10, 788–798
CoP/Ni_5P_4/CoP	71	58	Energy Environ. Sci. 2018, 11, 2246–2252
S-CoWP@(S,N)-C	67	/	ACS Energy Lett. 2018, 3, 1434−1442
N-P−Ni	25.8	34	ACS Energy Lett. 2019, 4, 805−810
Mo_5N_6	94	66	ACS Nano 2018, 12, 12761−12769
Pd_3Ru/C	42	/	ACS Catal. 2019, 9, 9614−9621
1D-RuO_2-CN_x	95	70	ACS Appl. Mater. Interfaces 2016, 8, 28678−28688
Pt_5/HMCS catalyst	46.2	48.1	Adv. Mater. 2019, 1901349
Ni, Zn dual-doped CoO NRs	53	47	Adv. Mater. 2019, 31, 1807771
Ir@CON	13.5	29	Adv. Mater. 2018, 30, 1805606
NiFeSe@NiSe|O@CC	62	48.9	Adv. Energy Mater. 2019, 9, 1802983
RuAu SAAs	24	37	Adv. Energy Mater. 2019, 1803913
CoP/NPC/TF	80	50	Adv. Energy Mater. 2019, 9, 1803970
S-MoS_2@C	155	99	Adv. Energy Mater. 2018, 1802553
Rh_2P	30	50	Adv. Energy Mater. 2018, 1703489
Ni_2P/MoS_2/N:RGO	149	60.2	Adv. Funct. Mater. 2019, 29, 1809151
FLNPC@MoP-NC/MoP-C/CC	69	52	Adv. Funct. Mater. 2018, 1801527
MoP/CNT	86	73	Adv. Funct. Mater. 2018, 1706523
RuP_2@NPC	52	69	Angew. Chem. Int. Ed. 2017, 56,11559 – 11564
CoP/Co-MOF	34	56	Angew. Chem. Int. Ed. 2019, 58,4679–4684
PdP_2@CB	35.4	42.1	Angew. Chem. Int. Ed. 2018, 57,14862–14867
NiRu@N–C	32	64	J. Mater. Chem. A,2018, 6,1376–1381
Rh–Rh_2O_3-NPs/C	63	70	J. Mater. Chem. A,2018, 6, 23531–23541
WC/W_2C@C NWs	56	59	J. Mater. Chem. A,2018, 6, 15395–15403
Pt/np-Co0.85Se	58	39	Nat Commun 2019, 10, 1743
Pt_1/N-C	46	36.8	Nat Commun 2020, 11, 1029
RuCo@NC	28	31	Nat Commun 2017, 8, 14969
Ru/CoFe-LDHs	198	39	Nat Commun 2019, 10, 1711
Ru@C_2N	17	38	Nature Nanotech 2017, 12, 441–446
Co-Fe-P nanotubes	86	66	Nano Energy 56 (2019) 225–233

Table S10. Summary of recently reported representative HER electrocatalysts in acidic electrolytes

Catalysts	Overpotential mV@10 mA cm^{-2}	References
RuO_2-300Ar	16	This work
IrP_2@NC	8	Energy Environ. Sci. 2019, 12 (3), 952–957.
Pt SASs/AG	12	Energy Environ. Sci. 2019, 12, 1000–1007
PtRu@RFCS	19.7	Energy Environ. Sci. 2018, 11, 1232–1239 |
Ni/WC@NC	53	Energy Environ. Sci., 2018, 11, 2114–2123
RuCoP	11	Energy Environ. Sci., 2018, 11, 1819–1827
CoP/Ni_5P_4/CoP	33	Energy Environ. Sci. 2018, 11, 2246–2252
CoMoP	41	Energy Environ. Sci. 2017, 10, 788–798
Li-$Pd_3P_2S_8$	52	Nat Catal. 2018, 1, 460–468
Mo_2TiC_2Tx–Pt_{SA}	30	Nat Catal. 2018, 1, 985–992
Mo-based and W-based molecular chalcoxides	114	Nat Commun 2019, 10, 370
Pt/np-$Co_{0.85}Se$	58	Nat Commun 2019, 10, 1743
Pt_1/N-C	19	Nat Commun 2020, 11, 1029
Ru@C_2N	13.5	Nature Nanotech 2017, 12, 441–446
CoP/Co-MOF	27	Angew.Chem. Int.Ed. 2019, 58,4679–4684
RuP_2@NPC	38	Angew. Chem. Int. Ed. 2017, 56, 11559–11564
PdP_2@CB	27.5	Angew. Chem. Int. Ed. 2018, 57, 14862–14867
Pt_5/HMCS	20.7	Adv. Mater. 2019, 1901349
$Ir_{25}Ni_{33}Ta_{42}$ MG nanofilm	99	Adv. Mater. 2019, 1906384
Pt/Ni/Ru	29.6	Adv. Mater. 2019, 31, 1805546
Ir@CON	13.6	Adv. Mater. 2018, 30, 1805606
CoP/NPC/TF	91	Adv. Energy Mater. 2019, 9, 1803970
S-MoS_2@C	136	Adv. Energy Mater. 2018, 1802553
Rh_2P	14	Adv. Energy Mater. 2018, 1703489
Ni_2P/MoS_2/N:RGO	39.5	Adv. Funct. Mater. 2019, 29, 1809151
FLNPC@MoP-NC/MoP-C/CC	74	Adv. Funct. Mater. 2018, 1801527
MoP/CNT	83	Adv. Funct. Mater. 2018, 1706523
1D-RuO_2-CN_x	93	ACS Appl. Mater. Interfaces 2016, 8, 28678−28688
S-CoWP@(S,N)-C	35	ACS Energy Lett. 2018, 3, 1434−1442
Ni–Pt films	90	Applied Catalysis B: Environmental 2020, 265 118597
NiRu@N–C	50	J. Mater. Chem. A 2018, 6,1376–1381
Rh–Rh_2O_3-NPs/C	13	J. Mater. Chem. A 2018, 6, 23531–23541
WC/W_2C@C NWs	69	J. Mater. Chem. A 2018, 6, 15395–15403
Co-Fe-P nanotubes	66	Nano Energy 2019, 56, 225–233

Table S11. Summary of recently reported representative HER electrocatalysts in neutral electrolytes

Catalysts	Overpotential mV@10 mA cm^{-2}	References
RuO_2-300Ar	29	This work
Pt/np-$Co_{0.85}Se$	55	Nat Commun 2019, 10, 1743
CoP/Co-MOF	49	Angew. Chem. Int. Ed. 2019, 58,4679–4684
PdP_2@CB	84.6	Angew. Chem. Int. Ed. 2018, 57,14862–14867
RuP_2@NPC	57	Angew. Chem. Int. Ed. 2017, 56,11559–11564
FLNPC@MoP-NC/MoP-C/CC	104	Adv. Funct. Mater. 2018, 1801527
MoP/CNT	102	Adv. Funct. Mater. 2018, 1706523
Rh_2P	38	Adv. Energy Mater. 2018, 1703489
Co-Fe-P nanotubes	138	Nano Energy 2019, 56, 225–233
CrO_x/Cu–Ni	48	Nat Energy 2019, 4, 107–114

Table S12. Summary of overall water-splitting electrocatalysts

Catalysts	Overpotential mV@10 mA cm^{-2}	References
RuO_2-300Ar//RuO_2-300Air	1.45 in 1 M KOH	This work
Ni NP|Ni–N–C	1.58 in 1 M KOH	Energy Environ. Sci. 2019, 12, 149–156
PdP_2@CB	1.72 in 1 M KOH	Angew. Chem. Int. Ed. 2018, 57, 14862–14867
S-CoWP@(S,N)-C//S-CoW@(S,N)-C	1.65 in 1 M KOH	ACS Energy Lett. 2018, 3, 1434−1442
Ni, Zn dual-doped CoO NRs	1.52 in 1 M KOH	Adv. Mater. 2019, 31, 1807771
NiFeSe@NiSe|O@CC	1.56 in 1 M KOH	Adv. Energy Mater. 2019, 9, 1802983
Pt/Ni/Ru	1.52 in 0.5 M H_2SO_4	Adv. Mater. 2018, 31, 1805546